Journal of Russian Laser Research, Volume 22, Number 2, 2001

THREE-BODY APPROXIMATION FOR THE INVESTIGATION OF EFIMOV STATES IN MOLECULAR SYSTEMS

S. A. Pozdneev

[1] *P. N. Lebedev Physical Institute, Russian Academy of Sciences, Leninskii Pr. 53, Moscow 117924, Russia*
e-mail: pozdneev@sci.lebedev.ru

Abstract

Using the three-body approximation with the well-known interatomic potential, the Efimov states in molecular systems are calculated. A mechanism of appearance and dissappearance of the Efimov states in the helium trimer in the three-body approximation is considered when the interatomic-interaction force is varied. Geometrical structure of these unusual quantum states are presented.

1. Introduction

The Efimov effect [1] is one of the most interesting and remarkable characteristics of three-body systems [2] compared with two-body systems. If at least two of the binary subsystems have s-state at zero energy with the corresponding scattering length A, the third particle interacts with the pair through an effective potential of the $1/R^2$-type,

$$R = r_1 + r_2 + r_3,$$

which provides an infinite number of three-body bound states

$$N \sim \ln\left(\frac{|A|}{|R|}\right).$$

The number becomes infinitely large also when the effective range approaches zero (in this limit, one has the Thomas effect [2]).

Although the Thomas effect is of interest from the theoretical point of view only, the Efimov states might be observed experimentally in a suitable weakly-bound three-body system. Candidates for observing the Efimov effect are Borromean [3], halo nuclei occurring in neutron drop line and molecular Ar_3-, Kr_3-, Xe_3-, Rn_3-, Ne_3-, Li_3-, He_2Li-, He_2Na-systems [3, 4], and atomic helium trimers [5–14].

Small He clusters (in particular, dimers and trimers) demonstrate a series of unusual quantum properties of fundamental interest. These properties can play an important role in describing the statistical behavior of collective modes in He gas at low temperature, as well as for the Bose–Einstein condensate and problems in laser physics connected with the light emission in the He_2^+ system [9–14].

The He_3 system is of considerable interest in various fields of physical chemistry and atomic and molecular physics. The study of the helium dimer and trimer provides important information for understanding the properties of helium liquid drops, superfluidity of He_3 films, etc. [4–7]. In addition, the

Manuscript submitted by the author in English on December 2, 2000.

1071-2836/01/2202-0175$25.00

proton–deuton- and neutron–deuton-systems [15–17] are probably unique systems where a direct manifestation of the Efimov effect [8, 15–17] can be observed since the binding energy of He_3 is extremely small even in the molecular scale [18]. For this reason, the He trimer is of certain interest for pure and applied sciences as well. Moreover, a theoretical investigation of the He trimer in the three-body approximation is based just on the same methods of the few-body-system theory that are used in solving the three-body nuclear problems.

From the standpoint of the general theory of few-body systems, the He trimer belongs to the three-body systems, which are the most difficult for the particular investigation due to its Efimov nature. That is why we consider the He trimer and other molecular systems in the cluster approximation as a system of simple three-field centers. Thus, the problem of three, for example, helium atoms can be considered as an ideal three-body quantum problem, since the He atoms are identical to neutral bosons with zero spin and analysis of this problem is complicated neither by the separation of spin–isospin variables nor by taking into account the Coulomb interaction.

There is a lot of experimental and theoretical studies of He clusters. However, most of the theoretical investigations consist merely in calculating the ground-state energy of He clusters mainly employing the variational methods [5, 14]. Besides, the methods based on hyperspherical expansions of the Schrödinger and Faddeev equations [2, 8, 15–17] in both momentum and coordinate representations were used. Also the Faddeev integral equations in the momentum representation were employed [2] while the results of [8, 15] were based on direct solution of the two-dimensional Faddeev differential equations in the configuration space.

As an experimental study, we would like to mention [3–11] where clusters consisting of a small number of noble-gas atoms were investigated. In spite of the fact that a lot of effort was undertaken to study various problems of molecular clusters, the He-trimer problem remains beyond the scope of through-and-through consideration. In particular, the elastic scattering phases of a helium atom on the helium dimer and break-up amplitudes were calculated [9]. These calculations were preceded only by the calculation of the characteristics of $He+He_2$-scattering at zero energy and estimation of the recombination rate.

As a matter of fact, we have already pointed out the main reason why the calculation of both excited and scattering states is especially difficult in the He-trimer system [3–15, 19]. First, the low energy of the He_2 dimer requires considering a fairly large domain in the configuration space with a characteristic size of hundreds of Å [5–9]. Second, according to [9] the very strong repulsive component in the He–He interaction produces considerable errors in the standard approximation of the three-atom Hamiltonian at short distances between the atoms [3–9].

In spite of the fact that the investigation of the He_3 system has a long history [3–15, 19], nevertheless some important physical problems are still far from clear. One of them deals with speculations on the Efimov-like nature of the He_3 bound states, namely, how many excited states can be proved by the best known model of interactions? Is it possible to estimate the difference in the number of bound states responsible for varying the model potential as limited by the accuracy of contemporary models? Another important question is connected with the characteristics of the He_3 bound states. Can the He_3 trimers influence the results of experimental measurement of the He_2-dimer characteristics? To solve the problem and answer the question pointed out, one should know such important characteristics of the He_3 cluster as the mean square radius of different states of the trimer and its geometric shape. The third question is connected with the influence of a hard core in the pairwise-potential interaction between helium atoms.

In this paper, we study the ^{4}He trimer by performing direct calculations of the He_3 bound states with different He–He model potentials [19]. Our approach is based on the Faddeev equations in the

configuration space due to the simplicity of numerical approximation of the Faddeev components in comparison with the wave function. In the case of Faddeev equations, the boundary conditions are also much simpler. In our case, for checking, the repulsive components of the He–He interaction at short distances between the atoms are approximated by a hard core. This allows one to investigate the He-trimer system within the framework of the mathematically rigorous method of solving a three-body problem in the boundary-condition model [2, 9, 16, 17]. An important advantage of such approach, which essentially diminishes computational errors, is the necessity to approximate (inside the core domain) the Laplacian operator only instead of the sum of the operator and huge repulsive components of the He–He potential. In [2, 9, 10, 15, 16], such an approach has been successfully applied for calculating not only the scattering states but also the binding energies of the ground and excited states of the various processes in nuclear, atomic, and molecular physics [17]. A detailed investigation has shown that the method proposed in [2, 9, 10] is appropriate for performing the few-body molecular calculations in the case where the repulsive components of interatomic interactions are of the hard-core nature.

There is a series of papers [3–14] where it was shown that the excited state of the He trimer is indeed initiated by the Efimov effect [1]. In these papers, various versions of He–He potential were employed [19]. However, the basic results of [3–15] on the excited state of the He trimer are the same — this state disappears if the interatomic potential is multiplied by the "amplification factor" Λ of the order of 1.2. More precisely, if this potential is multiplied by the increasing factor $\Lambda > 1$, then the following effect is observed. The difference $\epsilon_d(\Lambda) - E_t^1(\Lambda)$ between the dimer energy $\epsilon_d(\Lambda)$ and the energy of the trimer excited state $E_t^1(\Lambda)$ increases. The behavior of this difference changes drastically, and with further increase of Λ it decreases monotonically. At $\Lambda \approx 1.2$, the E_t^1-level disappears. Namely, such nonstandard behavior of the energy $E_t^1(\Lambda)$, when coupling between helium atoms becomes more and more strong, points to the Efimov nature of the trimer excited state. When Λ slightly decreases, the second excited state $E_t^2(\Lambda)$ appears in the trimer [3–15].

The aim of our paper is an interpretation of the trimer excited state up to its disappearance in the physical energy sheet and the study of the mechanism of new excited states arising. As the interatomic He–He interaction, we used the potential [19, 20] and established that for such He–He interaction the excited E_t^1-level of the trimer merged with the threshold ϵ_d at $\Lambda \approx 1.18$, and with further decrease of Λ it transformed into the first-order virtual level (a simple real pole of analytic continuation of the scattering matrix) located in a nonphysical energy sheet along the spectral interval between ϵ_d and the three-body threshold. We checked the position of this level at Λ increasing up to 1.5. Besides, we found that for $\Lambda < 1$ the excited level also originated from the first-order virtual levels, which constructed pairs. Before a pair of virtual levels appeared, a fusion of a pair of the first-order conjugate resonances (simple complex poles of the analytic continuation of the scattering matrix in the nonphysical energy sheet) has taken place and, as a result, the second-order virtual level arises.

As is be clear from [9], the resonances mentioned above are not, generally speaking, genuine resonances of the He trimer, since they are located outside the energy domain, for which we can rigorously prove the applicability of the method used for calculating the resonances. The resonances are found outside the domain of guaranteed applicability of the method of quasiresonances.

The paper is organized as follows.

Firstly, in Sec. 2 according to [2, 9] we describe the method of search for resonances in a three-body system using the Faddeev differential equations [2]. The main idea of the method consists in calculating the analytic continuation of the scattering-matrix components corresponding to different processes in a three-body system in the physical energy sheet using these equations. Particular attention is paid to

describing the specific parabolic domain on the physical energy sheet where one can continue analytically the function $S_0(z)$ by numerical solving the three-body differential equations in the coordinate space. For the potential used, the three-body resonances (including virtual levels) located in the nonphysical energy sheet [z-plane adjoined to the physical energy sheet along the interval $(\epsilon_d, 0)$] are roots of the function $S_0(z)$ in the physical energy sheet. Then, in Sec. 3 we describe briefly the numerical method [2–17] used to solve the problem of scattering states in the He trimer outside the domain of complex energies. In Sec. 3, we conclude by discussing the results of calculations.

2. Faddeev Differential Equations for Three-Body Systems

In the quantum theory of scattering for three-particle systems [2], the Faddeev differential equations are formulated by splitting the total wave function of the three particles into three parts, namely,

$$\Psi = \sum_{i=1}^{3} F_i,$$

with each part corresponding to all possible divisions of the system into noninteracting subgroups. For the He_3 system in the three-body approximation with pairwise potentials, these equations (after angular partial analysis) have the form

$$(H_{\lambda,l} - z)\, F_{aL}(x,y) = -V(x) \left[F_{aL}(x,y) + \sum_{a'} \int_{-1}^{+1} F_{a'L}(x',y')\, h^L_{aa'}(x',y',\eta)\; d\eta \right], \tag{1}$$

where

$$H_{\lambda,l} = -\frac{\partial^2}{\partial x^2} - \frac{\partial^2}{\partial y^2} + \frac{l(l+1)}{x^2} + \frac{\lambda(\lambda+1)}{y^2}\,, \tag{2}$$

with

$$z = E + i0, \qquad L = l + \lambda, \qquad a = (l,\lambda).$$

In the boundary-condition model, the right-hand side of Eqs. (1) is equal to zero for $x < c$, where c is the core size.

The functions $F_{aL}(x,y)$ are assumed to obey the boundary conditions

$$F_{aL}(x,y)\mid_{x=0} = 0, \qquad F_{aL}(x,y)\mid_{x=0} = 0, \tag{3}$$

and in the boundary-condition model they have the form

$$F_{aL}(c,y) + \sum_{a'} \int_{-1}^{+1} F_{a'L}(x',y')\, h^L_{aa'}(x',y')\, \eta\; d\eta = 0,$$

$$x' = \sqrt{\frac{x^2}{4} + \frac{3y^2}{4} - \frac{\sqrt{3}xy\eta}{2}}\,, \qquad y' = \sqrt{\frac{3x^2}{4} + \frac{y^2}{4} + \frac{\sqrt{3}xy\eta}{2}}\,.$$

At $\rho \to \infty$, the asymptotic conditions for the partial Faddeev components read

$$F_{aL}\mid_{\rho\to\infty} a_{aL,v} \sim \sum_v \psi_{l,v}(x) H_v\left(\sqrt{E - E_{2,l,v}}\right) + A_{aL}(\theta)\, \frac{\exp\,(i\sqrt{E}\rho) + i\pi L/2}{\sqrt{\rho}}\,, \tag{4}$$

where $\psi_{l,v}(x)$ are the partial wave functions of the pairwise subsystems with binding energy $\epsilon_{l,v}$,

$$\rho = \sqrt{x^2 + y^2}\,, \qquad \theta = \arctan\left(\frac{y}{x}\right),$$

$a_{aL,v}$ and $A_{aL}(\theta)$ are the elastic and break-up amplitudes, respectively, $H_v(x)$ is the spherical Hankel function, and the $h^L_{\alpha,\alpha'}$-function can be found in [2, 9, 10, 17].

While calculating the bound states at sufficiently large distances $x = R_x$ and $y = R_y$, one has [10]

$$\frac{\partial_x F_{aL}\,|_{x=R_x}}{F_{aL}|_{x=R_x}} = i\sqrt{\epsilon_v}, \qquad \frac{\partial_y F_{aL}\,\big|_{y=R_y}}{F_{aL}|_{y=R_y}} = i\sqrt{\epsilon_v - E}.$$

Consider the He_3 system in the state with the total angular momentum $L = 0$. In this case,

$$H_{\lambda,l} = H_{0,l} = -\frac{\partial^2}{\partial x^2} - \frac{\partial^2}{\partial y^2} + l(l+1)\left(\frac{1}{x^2} + \frac{1}{y^2}\right)$$

and the energy z can be both real and complex. At $L = 0$, the partial momentum l corresponds to the dimer and an additional atom. The momentum l can take only even values, $l = 0,\ 2,\ 4, \ldots$ The explicit form of the $h_{ll'}$ functions is presented in [2, 9, 10, 17]; here we deal with a finite number of Eqs. (1) assuming that $l \le l_{\max}$, where $l_{\max}$ is a certain fixed even number. The condition $0 \le l \le l_{\max}$ is equivalent to the assumption that the potential $V(x)$ acts only in the two-body states with $l = 0,\ 2, 4, \ldots, l_{\max}$. The spectrum of the Schrödinger operator for a system of three identical bosons with the potential $V(x)$ is denoted by σ_{3B}.

It is well known [2] that if the potential $V(x)$ is smooth and decreases at $x \to \infty$ along with its derivatives not slower than $x^{-3-\epsilon}$, $\epsilon > 0$, then the asymptotic conditions at $\rho \to \infty$ and/or $y \to \infty$ for the partial components of Eqs. (1) for the processes

$$1 + (2,3) \to \begin{cases} 1 + (2,3) & \text{elastic scattering} \\ 1 + (2,3)^* & \text{excitation} \\ (1,2)^* + 3 & \text{rearrangement with excitation} \\ (1,3)^* + 2 & \text{rearrangement with excitation} \\ 1 + 2 + 3 & \text{ionization, or decay into three free particles,} \end{cases}$$

at $z = E + i0$, $E > 0$, have the form

$$\begin{aligned} F_l(x,y;z) \;=\; & \delta_{l0}\psi_d(x)\left\{\sin\left(\sqrt{z-\epsilon_d}\,y\right) + \exp\left(i\sqrt{z-\epsilon_d}\,y\right)\left[a_0(z) + O(y^{-1/2})\right]\right\} \\ & + \frac{\exp\left(i\sqrt{z}\rho\right)}{\sqrt{\rho}}\left[A_l(z,\theta) + O(\rho^{-1/2})\right], \end{aligned} \tag{5}$$

where

$$\rho = \sqrt{x^2 + y^2}\,, \qquad \theta = \arctan\left(\frac{y}{x}\right),$$

and we assume that the He_2 dimer has only one bound state with energy ϵ_d ($\epsilon_d < 0$) and wave function $\psi_d(x)$.

The coefficient $a_0(z)$, $z = E + i0$ for $E > \epsilon_d$ is the elastic amplitude. The function $A_l(E, \theta)$ for $E > 0$ corresponds to the break-up amplitudes. This property ensures uniqueness of the solution of the boundary-condition problem (1)–(5) for the real scattering energy $E > \epsilon_d$ [2].

For the processes mentioned above, the component of the s-wave partial scattering matrix for a system of three particles is given (for real $z = E + i0$, $E > \epsilon_d$) by the expression [2]

$$S_0(z) = 1 + 2\, i a_0(z), \tag{6}$$

the scattering phases are of the form

$$\delta_0(p) = 0.5\,\mathrm{Im}\left[\ln\, S_0\left(\epsilon_d + p^2 + i0\right)\right], \qquad p > 0,$$

and the scattering length reads

$$L_{\mathrm{sl}} = -\frac{\sqrt{3}}{2}\,\lim_{p-0}\,\frac{a_0(p)}{p},$$

where p stands for momentum conjugate to the Jacobi variable y.

Following [9] our goal is to study the analytic continuation of the scattering matrix $S_0(z)$ into the complex plane (the physical energy sheet). As follows from the results of [2, 9], the roots of the function $S_0(z)$ in the physical energy sheet (z-plane) correspond to the location of the three-body resonances in the nonphysical energy sheet connected with the physical energy sheet by crossing the spectral interval $(\epsilon_d, 0)$. This statement is a particular case of more general statements regarding the three-body resonances [9] for the case of two-body potentials decreasing in the coordinate space not slower than exponentially. Assume that $V(x)$ is just a potential that falls exponentially and thus for all $x > 0$

$$\mid V(x) \mid \leq C \exp\left(-\mu x\right), \tag{7}$$

with some positive C and μ. For simplicity, we assume also that $V(x)$ is finite, i.e., $V(x) = 0$ for $x > r_0$, $r_0 > 0$. Looking ahead, note that, in fact, in our numerical calculations for the $^4\mathrm{He}_3$ system at complex energies, we take a "cutoff" of the interatomic He–He potential with a sufficiently large radius r_0.

It is well known that different representations of the same holomorphic function (for instance, either by a series or an integral) allow one to describe this function only in some parts of its Riemann surface. The description of holomorphic domains for different truncations of the total three-body scattering matrix in the physical energy sheet was based on the use of Faddeev integral equations in the momentum representation [2]. We employed the Faddeev equation in the configuration space. Therefore, it is necessary to perform (independently of [2]) the investigation of domains in the physical energy sheet where we can analytically continue the Faddeev components $F_l(x, y; z)$ and the amplitudes $a_o(z)$ and $A_l(z, \theta)$ just using the configuration-space techniques.

Let us list briefly the main results of the investigation [9] obtained for the three-body system under the assumption (7). To formulate the results, we distinguish the following three domains in the complex plane C.

(i) The domain $\prod^{\Psi}$ where the Faddeev components $F_l(x, y; z)$ and the wave function Ψ_l can be analytically continued in z-plane, so that the differences

$$\Phi_l(x, y; z) = F_l(x, y; z) - \delta_{l0}\psi_d(x) \sin\left(\sqrt{z - \epsilon_d}\, y\right) \tag{8}$$

at $z \in \prod^{\Psi} \setminus \sigma_{3B}$ turn out to be elements of $L_2(R_+^2)$. This domain is described by the inequality

$$\operatorname{Im}\sqrt{z-\epsilon_d} < \min\left[\frac{\sqrt{3}\mu}{2}, \sqrt{3}\sqrt{|\epsilon_d|}\right]. \tag{9}$$

For fixed x and y, the functions $\Phi_l(x,y;z)$ are continuous in the z-plane up to the rims of the cut along the continuous spectrum $[\epsilon_d, +\infty)$.

(ii) The domain $\prod^{A}$ where both the elastic scattering amplitude a_0 and break-up amplitudes $A_l(z,\theta)$ can be analytically continued in the z-plane, $z \not\subset \sigma_{3B}$, provided the functions $F_l(x,y;z)$ obey the asymptotic formula (5). This domain is described by the inequalities

$$\operatorname{Im}\sqrt{z} + 0.5\operatorname{Im}\frac{\sqrt{z-\epsilon_d}}{2} < \sqrt{3}\,\frac{\sqrt{|\epsilon_d|}}{2} \tag{10}$$

and

$$\operatorname{Im}\sqrt{z} + \sqrt{z-\epsilon_d} < \frac{\sqrt{3}\mu}{2}. \tag{11}$$

(iii) The domain $\prod^{S}$ is the most interesting, where the analytic continuation in the z-plane, $z \not\subset \sigma_{3B}$, can be done only for the elastic scattering amplitude [and consequently, for the scattering matrix $S_0(z)$]; the analytical continuability for the break-up amplitude $A_l(z,\theta)$ in the whole domain is not required. The $\prod^{S}$-set is a geometric locus of points obeying the inequality

$$\operatorname{Im}\sqrt{z-\epsilon_d} < \min\left[\frac{\sqrt{|\epsilon_d|}}{\sqrt{3}}, \frac{\sqrt{3}\mu}{2}\right]. \tag{12}$$

For the $\prod^{\Psi}$, $\prod^{A}$, and $\prod^{S}$-domains, the following chain of inclusionsis valid:

$$\overset{\Psi}{\prod} \subset \overset{A}{\prod} \subset \overset{S}{\prod}.$$

Note here that a condition of the type (9) or (12)

$$\operatorname{Im}\sqrt{z-a} < \sqrt{b}, \qquad a \in R, \qquad b > 0 \tag{13}$$

is equivalent to the inequality

$$\operatorname{Re} z > a - b + \frac{(\operatorname{Im} z)^2}{4b}. \tag{14}$$

Therefore, for $\mu \le 2\sqrt{|\epsilon_d|}$, the $\prod^{\Psi}$-set is a domain bounded by the parabola

$$\operatorname{Re} z > -|\epsilon_d| - \frac{3\mu^2}{4} + \frac{(\operatorname{Im} z)^2}{3\mu^2}. \tag{15}$$

For $\mu > 2\sqrt{|\epsilon_d|}$, the $\prod^{\Psi}$-set is the domain

$$\operatorname{Re} z > -4\,|\epsilon_d| + \frac{(\operatorname{Im} z)^2}{12|\epsilon_d|}. \tag{16}$$

Analogously, if $\mu \le 2\sqrt{|\epsilon_d|}/3$, then the $\prod^S$-domain is described by inequality (15); and for $\mu > 2\sqrt{|\epsilon_d|}/3$, by the inequality

$$\mathrm{Re}\, z > -\frac{4\,|\epsilon_d|}{3} + 3\,\frac{(\mathrm{Im}\, z)^2}{4\,|\epsilon_d|}\,. \tag{17}$$

As for the curves connecting domains (10) and (11), we only notice that their orders with respect to the variables $\mathrm{Re}\, z$ and $\mathrm{Im}\, z$ are higher than the second. It is easy to check that each curve is closed, symmetric with respect to the real z-axis, and crosses this axis only once. For the first curve, this cross occurs at $z = 3\epsilon_d/4$, the slope of the tangent at the cross point being independent of ϵ_d,

$$\frac{d\,\mathrm{Re}\, z}{d\,\mathrm{Im}\, z}\,|_{\mathrm{Im}\, z=\pm 0} = \pm\frac{\sqrt{3}}{2}\,.$$

At $\mathrm{Re}\, z \to \infty$, the boundaries (10) and (11) are asymptotically approximated by parabolas of the type (14) with coefficients a and b, which can be calculated explicitly.

To prove the assertion (i) concerning the $\prod^\Psi$-domain, note that the functions Φ_l given by formulas (8) satisfy the equations

$$[H_{0,l} + V(x) - z]\,\Phi_l(x,y;z) + V(x)\sum_{l'}\int_{-1}^{+1} h_{ll'}(x,y,r)\Phi_l(x',y';z)\;dr = \chi_l(x,y;z), \tag{18}$$

where

$$\chi_l(x,y;z) = -V(x)\int_{-1}^{+1} h_{0l}(x,y,r)\psi_d(x')\sin\left(\sqrt{z-\epsilon_d}\,y'\right).$$

Obviously, the functions $\chi_l(x,y;z)$ fall exponentially at $\rho \to \infty$.

Moreover, for all directions $0 \le \theta \le \pi/2$, the uniform estimate

$$\chi_l(x,y;z)_{\rho\to\infty} = O\Big(\exp\left(-\alpha\rho\right)\Big)$$

is valid with

$$\alpha = \min\left[\frac{\sqrt{3}\mu}{2} - \mathrm{Im}\,\sqrt{z-\epsilon_d},\;\frac{\sqrt{3}|\epsilon_d|}{2} - \mathrm{Im}\,\sqrt{z-\epsilon_d}\right].$$

Consequently, if the condition (9) holds, then the inhomogeneous terms $\chi_l(x,y;z)$ considered as functions of the variables x and y at fixed z are elements of $L_2(R_+^2)$. At the same time, the terms $\chi_l(x,y;z)$ turn out to be holomorphic functions of $z \in \prod^\Psi$ with respect to the $L_2(R_+^2)$-norm.

In the problem under consideration, the spectrum of the matrix operator determined by (18) with the boundary conditions (3) [consisting of the vectors $\Phi = (\Phi_1, \Phi_2, \ldots, \Phi_{l_{\max}})$] coincides with the spectrum σ_{3B} of the corresponding three-boson Schrödinger operator with the two-body potentials $V(x)$ acting on the states with $l = 0, 2, 4, \ldots, l_{\max}$ only. This means that for any energy $z \in \prod^\Psi$ (outside the spectrum σ_{3B}) the inhomogeneous system (18) is uniquely solvable in a class of the functions $\Phi \in L_2(R_+^2)$ $l = 0, 2, 4, \ldots, l_{\max}$. Since outside the σ_{3B}-set the resolvent of the Faddeev operator is a holomorphic operator (valued function of the z-variable), each of the $\Phi_l(z)$-components of the solution to Eq. (18) is also a holomorphic function of $z \in \prod^\Psi \setminus \sigma_{3B}$. The bound-state energies of the three-boson system under consideration turn out to be the first-order poles for $\Phi_l(z)$. Thus, the Faddeev partial components F_l admit an analytic continuation in the z-plane in the form (8) into the domain $\prod^\Psi \setminus \sigma_{3B}$.

Proving assertions (ii) and (iii) concerning domains $\prod^S$ and $\prod^A$ is rather cumbersome. This is why we present here only the main steps. Note that the proof is standard [2] based on the method of integral equations. First, Eqs. (18) are rewritten in the form of the Faddeev partial integral equations. To do this, it is sufficient to reverse the operators $H_{0,l} + V(x) - z$ in Eq. (18). Since the variables x and y in H_{0l} are separated, the kernels

$$4R_v^l(X, X', z), \qquad X = (x, y), \qquad X' = (x', y')$$

of the corresponding resolvents

$$R_v^l(z) = (H_{0,l} + V - z)^{-1}$$

are explicitly expressed in terms of the two-body problem. Analytic properties of the z-variable and coordinate asymptotics of the kernels $R_v^l(X, X', z)$ are well known [2]. Iterations first improve and stabilize the asymptotic properties of the iterated kernels and inhomogeneous terms of the Faddeev equations. Further, it turns out that for $z \not\subset [\epsilon_d, \infty]$ the iterated kernels are represented by sums of exponentially decreasing terms, which provided (in certain regions of the configuration space) an explicit asymptotic factorization with respect to X and X'. Since we are working in the domain where $\chi_l(z) \in L_2(R_+^2)$, the corresponding asymptotic factors of these terms (among asymptotics of iterations of inhomogeneous terms) determine the coordinate asymptotics of the $\Phi_l(x, y, z)$-functions. Therefore, finally, we are able to determine the geometric locus of the z-points in a complex plane for which there exists a (nonempty) set in the configuration space such that the leading term of the coordinate asymptotics of the $\Phi_l(x, y, z)$-function in this set represents a term of the form $a_0(z)\psi_d(x) \exp\left(i\sqrt{z - \epsilon_d}y\right.$ and thus, for these z-points, the scattering matrix $S_0(z)$ is well defined. This geometrical locus is just the $\prod^S$-domain. In this domain, at $y \to \infty$ and/or $\rho \to \infty$, the $\Phi_l(x, y, z)$-functions admit the asymptotic representation

$$\begin{aligned} F_l(x, y; z) &= \delta_{l0}\psi_d(x)\left\{\exp\left(i\sqrt{z - \epsilon_d}y\right)\left[a_0(z) + o(1)\right] + f_0(y, z)\right\} \\ &\quad + \frac{\exp\left(i\sqrt{z}\rho\right)}{\sqrt{\rho}}\left[A_l(z, \theta) + o(1)\right] + F_{1,l}(x, y, z), \end{aligned} \tag{19}$$

with

$$f_0(y, z)_{y\to\infty} = O\Big(\exp -\alpha_0(z)y\Big), \qquad F_{1,l}(x, y, z)_{\rho\to\infty} = O\Big(\exp -\alpha_1(z)\rho\Big), \tag{20}$$

where

$$\alpha_0(z) = \frac{\sqrt{3|\epsilon_d|} - \operatorname{Im}\sqrt{z - \epsilon_d}}{2} \tag{21}$$

and

$$\alpha_1(z) = \min\left[\alpha_0(z),\ \frac{\sqrt{3}\mu}{2} - \operatorname{Im}\sqrt{z - \epsilon_d},\ \operatorname{Im}\sqrt{z}\right]. \tag{22}$$

In the parabolic vicinity of the y-axis, the $F_{1,l}$-functions are also subjected to the asymptotic estimates

$$F_{1,l}(x, y, z)\,|_{y\to\infty,\, x<y^v} = O\Big(\exp -\alpha_0(z)y\Big), \qquad v < 1. \tag{23}$$

As for the $\prod^A$-domain, the leading asymptotic term of each of the $F_{1,l}$-functions for $z \in \prod^A$ is a spherical wave $\left[\exp\left(i\sqrt{z}\rho\right)\right]/\sqrt{\rho}$, with the amplitude $A_{1,l}(z, \theta)$ being a differentiable function of the angle θ. Therefore, for $z \in \prod^S$, the $F_{1,l}$-term in (19) can be added to the asymptotic term with a spherical

wave preceding $F_{1,l}$. In the $\prod^S$-domain, and hence, in a narrower $\prod^A$-domain, the condition (20) holds. Consequently, for $z \in \prod^A$, the $F_{1,l}$-components do obey the standard asymptotic conditions similar to (5).

Therefore, for any $v < 1$, the dominant term of the asymptotics of the function $\Phi_0(x, y, z), z \in \prod^S \setminus \sigma_{3B}$ at $x < y^v$ reads as $a_0(z)\psi_d(x)\exp(i\sqrt{z-\epsilon_d}y)$ for $y \to \infty$. This means that for $z \in \prod^S \setminus \sigma_{3B}$ it is always possible to separate explicitly the elastic scattering amplitude $a_0(z)$ by solving Eqs. (1) and thus to construct the analytic continuation of the scattering matrix $S_0(z)$.

Outside the $\prod^S$-domain, the numerical construction of $S_0(z)$ by means of solving the Faddeev differential equations is, in general, impossible, since for $x < y^v$, $v < 1$ both functions $f_0(x, z)$ and $F_{1,l}(x, y, z)$, $z \not\subset \prod^S$ have terms decreasing slower than $\exp(i\sqrt{z-\epsilon_d}y)$ at $y \to \infty$.

In the case of potentials with a hard core, the partial differential equations for a system of three identical bosons at $L = 0$ have the form

$$[H_{0l} - z]F_l(x, y) = \begin{cases} -V(x)\Psi_l(x, y) & x \geq c, \\ 0 & x \leq c, \end{cases} \tag{24}$$

where $c > 0$ is the core size. The partial wave functions $\Psi_l(x, y)$ are expressed through the partial components $F_l(x, y)$ by formula (4). The $F_l(x, y)$-components satisfy the boundary conditions (3). The two-body central potential $V(x)$ acts only beyond the core region. Assume, as before, that $V(x)$ falls not slower than exponentially at $x \to \infty$ and hence it satisfies the condition (7) for some $c > 0$ and $\mu > 0$.

The fundamental difference between the model with a hard core and those with smooth potentials is that the $F_l(x, y)$-functions in the former model satisfy the auxiliary boundary conditions

$$F_l(x, y) + \sum_{l'} \int_{-1}^{+1} F'_l(x', y')h_{ll'}(c, y, r)\, dr = 0, \tag{25}$$

which require that the wave functions $\Psi_l(x, y)$ vanish at the boundary $x = c$ of the core region. It can be shown that, in fact, the conditions (25) force the wave functions (4) to vanish also inside the core domain at all energies, except a certain countable set of real values of z [2, 8].

Asymptotic conditions for the partial Faddeev components $F_l(x, y, z)$ (for the processes mentioned above) of the scattering wave functions at $\rho \to \infty$ and/or $y \to \infty$ are of the form (5). The only difference is that the dimer wave function ψ_d is considered as zero in the core region (for $0 \leq x \leq c$).

In the hard-core model, all assertions concerning the holomorphic domain of the $\Psi_l(x, y)$-functions and the scattering matrix $S_0(z)$ in the z-plane still hold true.

Above we have already noticed that the roots of $S_0(z)$ in the physical energy sheet (z-plane) correspond to the location of three-body resonances in the nonphysical energy sheet [adjoining the physical energy sheet along the spectral interval $(\epsilon_d, 0)$].

In the case under consideration, this statement is a direct consequence of the unitarity of the scattering matrix $S_0(z)$ for $z = E + i0$, $\epsilon_d \leq E \leq 0$,

$$S_0(E + i0)\overline{S_0(E + i0)} = 1. \tag{26}$$

Indeed, as we have established, the functions are holomorphic functions $z \in \prod^\Psi \setminus \sigma_{3B}$. Since the boundary-condition problem (1)–(5) is uniquely solvable, one can easy verify that the boundary values $\Psi_l(x, y, E + i0)$ and $\Psi_l(x, y, E - i0)$ for these functions on the rims of the cut along $[\epsilon_d, +\infty)$ are related as follows:

$$\Phi_l(x, y, E + i0) = -\overline{\Phi_l(x, y, E - i0)}, \tag{27}$$

since, on the one hand, their asymptotics (19) at $y \to \infty$ and/or $\rho \to \infty$ have the same structure and, on the other hand,

$$\chi_l(x, y, E + i0) = -\chi_l(x, y, E - i0) = -\overline{\chi_l(x, y, E - i0)},$$

since

$$\sin\sqrt{E - \epsilon_d + i0}y = -\sin\sqrt{E - \epsilon_d - i0}y = -\overline{\sin\sqrt{E - \epsilon_d - i0}y}.$$

Consequently,

$$a_0(E + i0) = -\overline{a_0(E - i0)} \tag{28}$$

and

$$S_0(E + i0) = \overline{S_0(E - i0)}, \qquad E > \epsilon_d. \tag{29}$$

Therefore, from (26) it follows that for $\epsilon_d \le E \le 0$

$$S_0(E + i0) = [S_0(E - i0)]^{-1} \qquad \text{and} \qquad S_0(E - i0) = [S_0(E + i0)]^{-1}.$$

This means that the function $S_0(E + i0)$ is continued through the cut $[\epsilon_d, 0]$ into the region $\operatorname{Im} z < 0$ as $S_0^{-1}(z)$. In a similar manner, $S_0(E - i0)$ is continued into the region $\operatorname{Im} z > 0$ as $S_0^{-1}(z)$. From this consideration, it follows that the scattering matrix $S_0(z)$ admits

(1) an analytic continuation at least into the $\prod^S$-domain (nonphysical energy sheet) connected with the physical energy sheet by crossing the interval $[\epsilon_d, 0]$,

(2) the value of the continued function $S_0(z)$ at $z \in \prod^S$ in the nonphysical energy sheet coincides with the value of $S_0^{-1}(z)$ at the same z but in the physical energy sheet.

Recall that the z-points on the nonphysical energy sheet are called resonances (where the analytically continued scattering matrix possesses poles). z-Resonances with $\operatorname{Im} z = 0$ and $\operatorname{Re} z < \epsilon_d$ are called virtual levels.

Thus, we have presented a simple proof of the fact that the resonances (including the virtual levels) corresponding to the poles of the analytically continued scattering matrix $S_0(z)$ in the nonphysical energy sheet (connected with the physical energy sheet by crossing the spectral interval $[\epsilon_d, 0]$) are roots of this matrix on the physical energy sheet. At the same time, the poles of the function $S_0(z)$ on the physical energy sheet correspond to a bound state of the three-boson system under consideration.

Concluding, it is worth noting that from (28) it follows that

$$a_0(z) = -\overline{a_0(z)}$$

and hence

$$\overline{S_0(z)} = S_0(z) \tag{30}$$

for any $z \in \prod^S$. This means that the roots of the function $S_0(z)$ are located symmetrically with respect to the real axis.

3. Numerical Method and the Results of Calculation

For the numerical solution of Eqs. (1) with boundary conditions, the method proposed in [2, 9, 10, 15–17] was usually used. As the pairwise potentials we studied the HFDHE2, HFD-B, HFDID, LM2M1, LM2M2, and TTYPT potentials [19] with parameters describing the properties of the investigated molecules in detail [20].

TABLE 1. Energy, Scattering Length, Mean Radius, and Mean Square Radius of the He_2 Molecule

Potential	E_{He_2}, mK	l_{sl}, Å	$\langle r_{He_2}\rangle$, Å	$\langle r^2_{He_2}\rangle^{1/2}$, Å
HFDHE2	−0.8301	89.30	64.21	88.18
HFD-B	−1.6854	88.40	46.18	62.71
HFD-ID	−0.4023	79.10	91.50	126.73
LM2M1	−1.2091	101.10	53.85	73.54
LM2M2	−1.3035	101.25	52.00	70.93
TTYPT	−1.3123	100.05	51.84	70.71

TABLE 2. Energy, Scattering Length, Mean Radius, and Mean Square Radius of the He_2 Molecule in the BCM Approximation

Potential	E_{He_2}, mK	l_{sl}, Å	$\langle r_{He_2}\rangle$, Å	$\langle r^2_{He_2}\rangle^{1/2}$, Å
HFDHE2	−0.8301	123.87	64.20	88.15
HFD-B	−1.6841	88.48	46.18	62.71
HFD-ID	−0.4009	81.15	96.54	125.83
LM2M1	−1.2891	101.10	53.85	73.54
LM2M2	−1.3035	100.25	56.01	71.83
TTYPT	−1.3096	100.05	54.75	70.81

TABLE 3. Energy, Contribution of the Cluster Wave to the Faddeev Component, Scattering Length, Mean Radius, and Mean Square Radius of the He_3 Molecule

Potential	E_{He_3}, mK	$\|f_c\|^2$	L_{sl}, Å	$\langle r_{He_3}\rangle$, Å	$\langle r^3_{He_2}\rangle^{1/2}$, Å
HFDHE2	−0.1171	0.2094	140	5.65	6.46
HFD-B	−0.1330	0.2717	137	5.48	6.23
HFD-ID	−0.1061	0.1555	139	5.80	6.64
LM2M1	−0.1247	0.2412	132	5.57	6.35
LM2M2	−0.1264	0.2479	131	5.55	6.32
TTYPT	−0.1264	0.2487	130	5.56	6.33

TABLE 4. Energy, Contribution of the Cluster Wave to the Faddeev Component, Scattering Length, Mean Radius, and Mean Square Radius of the He_3 Molecule in the BCM Approximation

Potential	E_{He_3}, mK	$\|f_c\|^2$	L_{sl}, Å	$\langle r_{He_3}\rangle$, Å	$\langle r^3_{He_2}\rangle^{1/2}$, Å
HFDHE2	−0.1170	0.2095	138	5.65	6.46
HFD-B	−0.1329	0.2717	135	5.48	6.23
HFD-ID	−0.10612	0.1555	134	5.80	6.64
LM2M1	−0.12465	0.2412	130	5.57	6.35
LM2M2	−0.12641	0.2479	131	5.55	6.32
TTYPT	−0.12640	0.2487	131	5.56	6.33

TABLE 5. Energy, Contribution of the Cluster Wave to the Faddeev Component, Scattering Length, Mean Radius, and Mean Square Radius of the He_3^* Molecule

Potential	$E_{He_3^*}$, mK	$\|f_c^*\|^2$	L_{sl}, Å	$\langle r_{He_3^*}\rangle$, Å	$\langle r^3_{He_3^*}\rangle^{1/2}$, Å
HFDHE2	−1.6653	0.9077	134	55.26	66.25
HFD-B	−2.743	0.9432	135	48.33	57.89
HFD-ID	−1.0612	0.8537	140	62.75	75.38
LM2M1	−2.1550	0.9283	129	51.53	61.74
LM2M2	−2.2713	0.9319	131	50.79	60.85
TTYPT	−2.2806	0.9323	131	50.76	60.81

TABLE 6. Energy, Contribution of the Cluster Wave to the Faddeev Component, Scattering Length, Mean Radius, and Mean Square Radius of the He_3^* Molecule in the BCM Approximatrion

Potential	$E_{He_3^*}$, mK	$\|f_c^*\|^2$	L_{sl}, Å	$\langle r_{He_3^*}\rangle$, Å	$\langle r^3_{He_3^*}\rangle^{1/2}$, Å
HFDHE2	−1.6765	0.9078	135	56.22	67.11
HFD-B	−2.7458	0.9439	135	48.31	58.00
HFD-ID	−1.1061	0.8597	136	62.87	76.13
LM2M1	−2.2585	0.9323	132	52.41	62.04
LM2M2	−2.2801	0.9319	131	50.79	61.05
TTYPT	−2.2885	0.9339	131	51.23	60.89

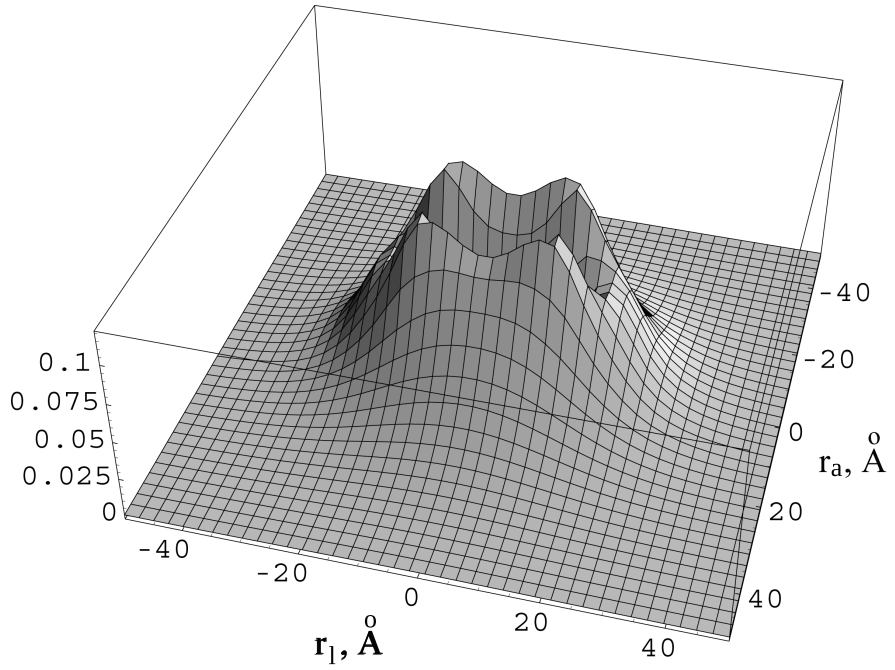

Fig. 1. Conditional single-particle density function of the He_3 ground state.

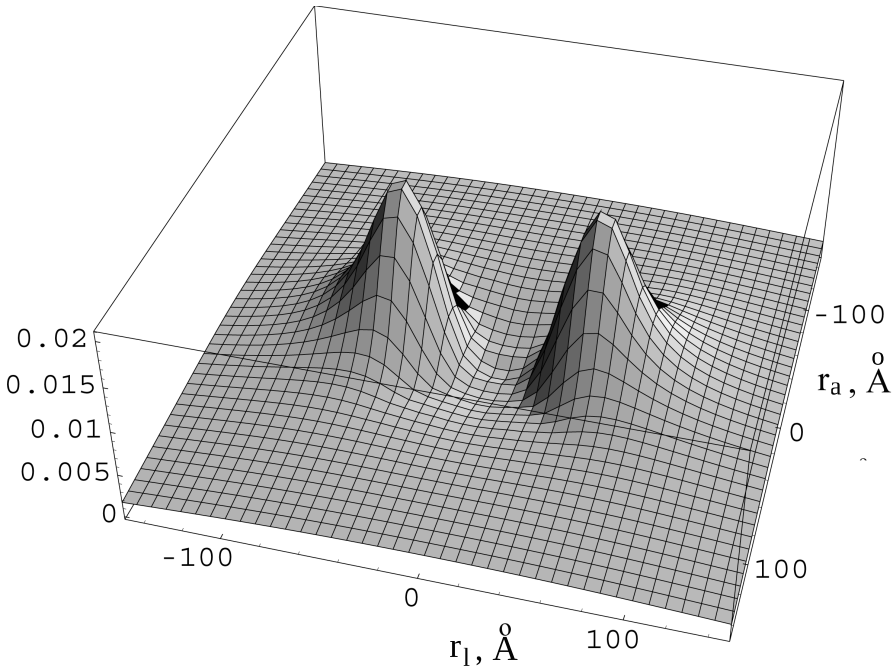

Fig. 2. Conditional single-particle density function of the He_3^* excited state (HFDHE2 potential).

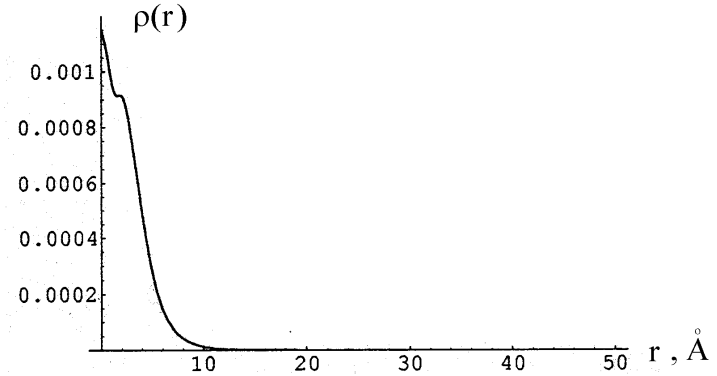

Fig. 3. Density function of the He_3 ground state.

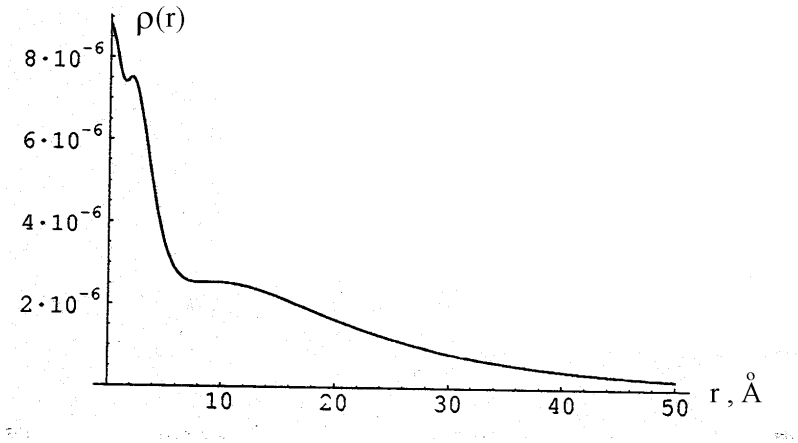

Fig. 4. Density function of the He_3 excited state.

The results of calculations — binding energy for the He_2-, He_3-, and He_3^*-systems both in the boundary-condition model (BCM) and without BCM are presented in Tables 1–5.

For the interpretations of the geometric structure of He_3, Figs. 1–4 present the results of calculations of the density functions determined as [10]

$$\varrho(\vec{r}_1) = \int |\Psi(\vec{r}_1, \vec{r}_2, \vec{r}_3)|^2 \, d\vec{r}_2 \, d\vec{r}_3,$$

$$\Psi(\vec{r}_1, \vec{r}_2, \vec{r}_3) = \left\{ F(x, y, z') + xy \left[\frac{F(x^+, y^+, z'^+)}{x^+ y^+} + \frac{F(x^-, y^-, z'^-)}{x^- y^-} \right] \right\} \frac{1}{2\pi xy},$$

where

$$z' = \frac{(\vec{x}', \vec{y}')}{x'y'}, \qquad x^{\pm} = \left(\frac{x^2}{4} + \frac{3y^2}{4} \pm \frac{\sqrt{3}xyz'}{2} \right)^{1/2}, \qquad y^{\pm} = \left(\frac{3x^2}{4} + \frac{y^2}{4} \pm \frac{\sqrt{3}xyz'}{2} \right)^{1/2},$$

$$x = x\left(\vec{r}_1, \vec{r}_2, \vec{r}_3\right), \qquad y = y\left(\vec{r}_1, \vec{r}_2, \vec{r}_3\right), \qquad z = z\left(\vec{r}_1, \vec{r}_2, \vec{r}_3\right).$$

If symmetry of the He_3 molecule is taken into account, the density function reads

$$\varrho(r) = \frac{\sqrt{3}}{4\pi^2 r^2} \int |\Psi(x, r\sqrt{3}, z')2\pi xy|^2 \, dx \, dz'.$$

Three-dimensional plots of the function $\varrho\Big[(r_l^2+r_a^2)^{1/2},\ \cos\arctan\left(r_l/r_a\right)\Big]$ corresponding to the ground and excited states of the He_3- and He_3^*-systems with the HFDHE2, HFD-B, HFDID, LM2M1, LM2M2, and TTYPT potentials are presented in Figs. 1–4, where $r_l = rz'$ is the projection of the position of particle 1 on the axis connecting the other particles, and

$$r_a = \frac{z'}{|z'|}\left(1 - z'^2\right)^{1/2}$$

is the projection on the orthogonal axis. The density function of the ground state decreases rapidly in all directions, while the density function of the excited state has two distinguishable maxima demonstrating the linear structure of the He_3^* system, which has a simple physical explanation. The most probable position of a particle in the excited state is located in the vicinity of two other particles. At distances where the two particles are well separated, the third particle forms a dimer-like bound state with each of the two particles, and this interpretation agrees with the clusterization coefficient f_c determined as follows [10]:

$$f_c = \int F(x, y, z')\phi_{\mathrm{He}_2}(x) \, dx \, dz'.$$

The absolute values of the components $\phi_{000}(x, y, p)$ and $\phi_{220}(x, y, p)$ for $E = 1.4\,\mathrm{mK}$ are shown in Figs. 5 and 6. It is worth noting here that at large distances y the component $\phi_{000}(x, y, p)$ dominates in the incident plane wave $\Psi_{\mathrm{He}_2}(x)\sin py$; this can be explicitly observed in Fig. 5. However, such behavior does not characterize the partial $\phi_{220}(x, y, p)$-component, which differs significantly from zero only in the vicinity of the triple-collision point, because in this region the coupling between channels $l = \lambda = 0$ and $l = \lambda = 2$ [due to the integral terms of Eqs. (1)] is large. It is interesting that the structure of functions $\phi(x, y, p)$ and $F(x, y.z')$ practically does not depend on the interaction potentials considered in the energy range $\epsilon_{\mathrm{He}_2} < E < 3\,\mathrm{mK}$. All calculations were performed at the following parameters:

$$N_\theta = N_\rho = 700 - 1200 \qquad \text{and} \qquad \rho_{\max} = 800\,\text{Å}\,.$$

The contour diagram of the particle density in the intrinsic coordinate systems (with center of mass at the origin) for the ground (a) and excited (b) states of the He_3 system are presented in Fig. 7 where the distance scales are quite different. The triangular shape of the diagram for the ground state of the He_3 system in Fig. 7a is quite obvious but the diagram for the excited state (Fig. 7b) shows that the particle is located in the vicinity of the two other particles (compare with Fig. 2), which corresponds to the Efimov conditions, i.e., fairly large scattering lengths for at least two of the binary subsystems. Thus, Figs. 2 and 7 illustrate the structure of the Efimov state. The other Efimov states located higher can be found by scaling the axes [1].

A similar triangular structure arises in the case of calculations using the three-body approximation of ground and excited states of the Ne_3, Ar_3, Kr_3, Xe_3, Li_3, and $^{12}C_3$ systems. Results of the calculations with the HFD–B potential are given in Tables 7 and 8. Probably, for the $^{12}C_3$ system, the two other

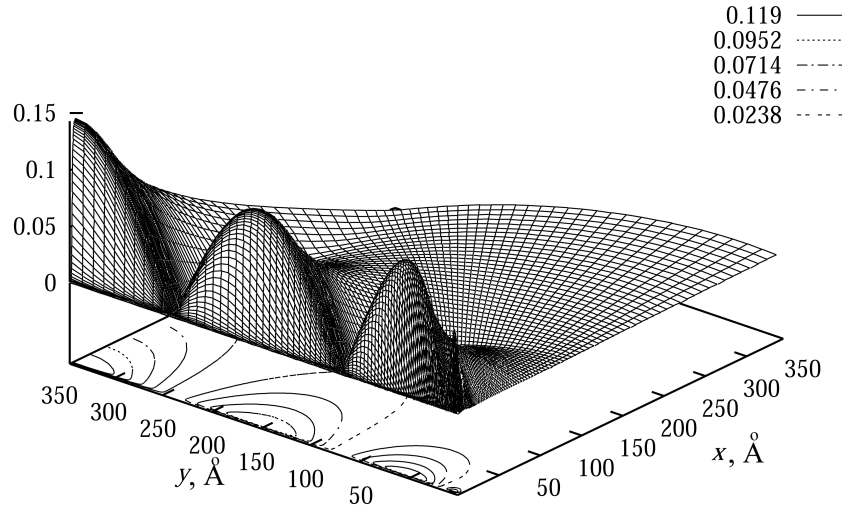

Fig. 5. Absolute value of the Faddeev component $F_{000}(x, y, p)$ for the HFD-B potential at $E = +1.4\,\mathrm{mK}$.

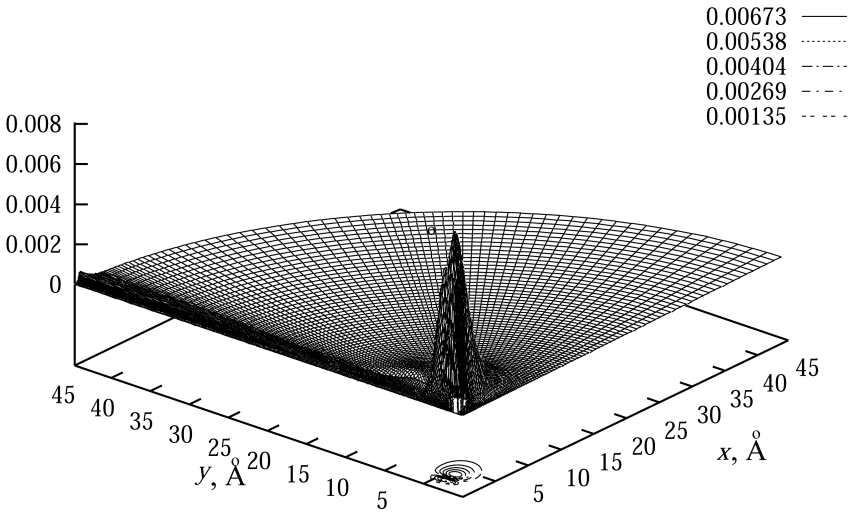

Fig. 6. Absolute value of the Faddeev component $F_{220}(x, y, p)$ for the HFD-B potential at $E = +1.4\,\mathrm{mK}$.

TABLE 7. Ground Energy of Diatomic Rare-Gas Molecules with the HFD-B Potential

Energy/Molecula	Ne_2	Ar_2	Kr_2	Xe_2	Rn_2
$E_{\text{theor.}} \times 10^6$, a.u.	178	394	619	854	9268
$E_{\text{exp.}} \times 10^6$, a.u.	135	446	629	874	-

TABLE 8. Ground and First Excited Energy of Three-Atomic Rare-Gas Molecules with the Pairwise HFD-B Potential (a.u.$\times 10^{-6}$)

Ne_3	Ne_3^*	Ar_3	Ar_3^*	Kr_3	Kr_3^*	Xe_3	Xe_3^*	Rn_3	Rn_3^*
398	330	1278	1215	1885	1811	2509	2438	30875	30801

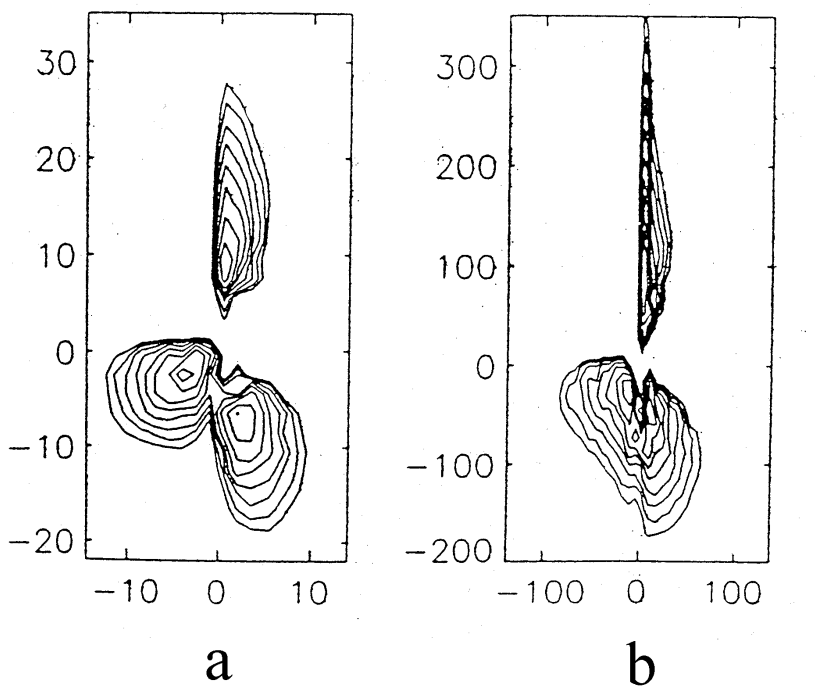

Fig. 7. Contour diagrams of the particle-density distributions for the ground and excited states of the He_3 system.

trimer states are fairly different from the almost linear configuration of the first excited state (interesting from the astrophysical point of view), which therefore is far from being any Efimov state.

The value of the parameter c (diameter of particles) is chosen small enough so that its further decrease is not remarkably sensitive to the influence on the dimer binding energy ϵ_d and the energy E_t^0 of the trimer ground state. Now we put $c = 1.5$ Å, unlike [8] where c was equal to 0.7 Å. The chosen value of c

precisely provides $\epsilon_d = -1.69\,\text{mK}$ and $E_t^0 = -0.96\,\text{m}$. In all our calculations r_0 was 100 Å.

Before making the numerical approximation of the system of Eqs. (1), (3), (24), (25), and (26) at $l_{\max} = 0$, we rewrite them in terms of Φ_0 functions, which are expressed in terms of the Faddeev component F_0 by relation (8). Note here that for $z \in \Pi^\Psi \setminus \sigma_{3B}$ the Φ_0 functions are square integrable in x and y. Therefore, these functions are uniquely determined by the asymptotic condition

$$\Phi_0(x, y, z)_{\rho\to\infty} \to 0,$$

which can be easily approximated and subjected to a computational program. For instance, one could require

$$\Phi_0(x, y, z)_{\rho=\rho_{\max}} = 0$$

at sufficiently large $\rho_{\max}$ and look for a numerical solution of the system of Eqs. (1), (3), (5), (24), and (25) satisfying this condition. Further, for $z \in \Pi^S$ one could (by penetrating far enough from $\rho_{\max}$ into the domain of smaller values of ρ) separate the elastic scattering amplitude $a_0(z)$, putting, e.g., $a_0(z) \sim \Phi_0(x, y, z) \exp -i\sqrt{z - \epsilon_d}\, y$, where the value of x corresponds to the maximum of the function $\psi_d(x)$. Such approach, however, appears ineffective in view of the relatively slow decrease of the exponentials $\exp -\sqrt{|\epsilon_d|}x$ and $\exp\left[-\text{Im}\,\sqrt{z - \epsilon_d}\, y\right]$, along with the decrease of the function $\exp\left(-\text{Im}\,\sqrt{z}\rho\right)$ in the energy domain of interest in the Π^S-domain. For a proper approximation of the condition (32), one has to take very large values of $\rho_{\max}$. This is precisely the reason why one should take into account the asymptotics of the function Ψ_0 at $x \to \infty$ or/and $y \to \infty$. The asymptotic formula (5) holds only for $z \in \Pi^S \setminus \Pi^A$. Indeed, when $z \in \Pi^S \setminus \Pi^A$, the leading term of the asymptotics of Φ_0 at $y \to \infty$ and $x < y^\nu$, $\nu < 1$, is given by the same expression $a_0(z) \exp -i\sqrt{z - \epsilon_d}\, y$ as in (5). Outside the parabola $x < y^\nu$ it is sufficient to require that the condition (32) be satisfied. The presence of the spherical wave $\exp i\sqrt{z}\rho/\sqrt{\rho}$ in (5) does not contradict this requirement. Therefore, the use of asymptotic condition (5) is justified even if $z \in \Pi^S \setminus \Pi^A$.

A detailed description of the method used for numerical solution of Eqs. (1), (24), and (25) is presented in [2, 9, 10, 15, 16]. Here we mention the main computation steps for a better understanding of the results.

While solving the boundary-condition problem (1), (3), (5), (24), and (25), we carried out its finite-difference approximation in polar coordinates ρ and θ. The grid was chosen in such a way that the points of intersection of arcs $\rho = \rho_i$, $i = 1, 2, 3, \ldots, N_\rho$ and rays $\theta = \theta_j$, $j = 1, 2, 3, \ldots, N_\theta$ with the line $x = c$ turn out automatically to be knots. The ρ_i points were chosen according to the formula

$$\begin{aligned} \rho_i &= \frac{ic}{N_c^\rho + 1}, \qquad i = 1, 2, 3, \ldots, N_c^\rho \\ \rho_{i+N_c^\rho} &= \sqrt{c^2 + y_i^2}, \qquad i = 1, 2, 3, \ldots, N_\rho - N_c^\rho, \end{aligned}$$

where N_c^ρ stands for the number of arcs inside the core domain, and

$$y_i = f(\tau_i)\sqrt{\rho_{N_\rho}^2 - c^2}, \qquad \tau_i = \frac{i}{N_\rho - N_c^\rho}.$$

The nonlinear monotonously increasing function $f(\tau)$, $0 < \tau < 1$, satisfying the conditions $f(0) = 0$, $f(1) = 1$, was chosen in the form

$$f(x) = \begin{cases} ax, & \text{for } x \in [0, x_0], \\ a_1 x + x^\nu, & \text{for } x \in [x_0, 1] \end{cases}.$$

The values of a_0, $a_0 > 0$ and a, $a_1 > 0$ are determined through x_0, ν from the continuity condition for $f(x)$ and its derivative in the x_0 point. As a rule, we took values of x_0 within 0.1 and 0.2. The value of power ν depends on the cut-off radius $\rho_{\max} = \rho_{N_\rho} = 50 - 5000$ Å and its range may be increased by 2–5 times.

The knots $\theta = \theta_j$, $j = 1, 2, 3, \ldots, N_\rho - N_c^\rho$, were taken according to $\theta_j = \arctan(y_j/c)$. The remaining knots θ_j, $j = N_\rho - N_c^\rho + 1, \ldots, N_\theta$, were chosen equidistantly. Such a choice of the grid was prescribed by the need to have a higher density of points in the region where the $\Psi_l(x, y, z)$ functions changed most rapidly, i.e., for small values of ρ and x in the asymptotic region. For this calculation, we used a grid of dimension $N_\theta = N_\rho = 700 - 1200$. The number of remaining knots of θ located in the core region N_c^ρ was usually equal to seven.

The finite difference approximation of Eqs. (24) and the boundary conditions (3), (3), (25) for the case $l_{\max} = 0$ reduces the problem to a system of $N_\theta N_\rho$ linear algebraic equations. The finite difference equations corresponding to the arc $i = N_\rho$ include initially the values of the unknown function on the arc $i = N_\rho + 1$. To eliminate these values, we express them through the Φ-function values on the arcs $i = N_\rho$ and $i = N_\rho - 1$ by using the asymptotic formula (5). The matrix of the resulting system of equations has a three-diagonal-block form [2, 8, 15]. Every block has the $N_\theta N_\theta$-dimension and consists of the coefficients at unknown values of the Φ-function in the grid knots belonging to a certain arc $\rho = \rho_i$. The main diagonal of the matrix consists of N_ρ blocks.

For the solution of the system of three-diagonal-block algebraic equations, we used the matrix-sweep method [21]. This allowed us to write the system matrix on the hard drive and to carry out all operations related to its inversion directly.

We searched for the resonances [roots of the $S_0(z)$-function on the physical energy sheet] and the bound-state energies (roots of the $S_0^{-1}(z)$-function for real $z < \epsilon_d$] of the helium trimer by using the complex version of the secant method [9, 21]. Within the framework of this method, the approximation of z_n to a root of a holomorphic function $f(z)$ was constructed from the two previous approximations z_{n-1} and z_{n-1} according to the formula

$$z_n = z_{n-1} - \frac{f(z_{n-1})(z_{n-1} - z_{n-2})}{f(z_{n-1}) - f(z_{n-2})}.$$

Because relation (30) implies the symmetry properties of the scattering matrix $S_0(z)$ with respect to the real axis, we performed all calculations of $S_0(z)$ only for $\operatorname{Im} z > 0$. We started by studying the graph surfaces of real and imaginary parts of the scattering matrix $S_0(z)$ in the domain of its holomorphy $\Pi^S \setminus \sigma_{3B}$. The root line of the function $\operatorname{Re} S_0(z)$ and $\operatorname{Im} S_0(z)$ was obtained for grid parameters as follows: $N_\theta = N_\rho = 700$ and $\rho = 700$. Both resonances [roots of $S_0(z)$] and bound-state energies [poles of $S_0(z)$] of the helium trimer were associated with the intersection points of the curves $\operatorname{Re} S_0(z) = 0$ and $\operatorname{Im} S_0(z) = 0$. If the roots or poles are simple, these curves intersect each other at right angles. Note that for real $z < \epsilon_d$ the $S_0(z)$-function is real and thus $\operatorname{Im} S_0(z) = 0$.

The caption points located outside the positions of four resonances [roots of the $S_0(z)$-function] were found just beyond the boundary of the Π^S-domain. As one might expect, the values of the $S_0(z)$ function at $z \in C \setminus \Pi^S$ and the positions of its roots in $C \setminus \Pi^S$ turn out to be unstable and strongly dependent on the value of the cut-off radius $\rho_{\max}$, whereas the dependence on the number of knots was weak. In

particular, for $\rho_{\max} = 400\,\mathring{A}$, the closest to the real axis quasiresonance is located at the point

$$\begin{aligned}
&(-1.96 + i\,1.82)\ \text{mK}, \qquad \text{if} \qquad N_\theta = N_\rho = 400,\\
&(-1.91 + i\,1.85)\ \text{mK}, \qquad \text{if} \qquad N_\theta = N_\rho = 600,\\
&(-1.90 + i\,1.86)\ \text{mK}, \qquad \text{if} \qquad N_\theta = N_\rho = 700.
\end{aligned}$$

The same quasiresonance calculated for $\rho_{\max} = 700$ Å is located at the point $(-2.35 + i\,0.98)$ mK.

If $N_\theta = N_\rho$ are fixed and equal to 600, $\rho_{\max}$ increases up to 900 Å, and this point shifts to $(-2.44 + i\,0.66)$ mK.

All the above-mentioned comments [9] regarding the instability of the $S_0(z)$ function (its values and the position of the roots beyond the Π^S-domain) have no relation to its pole at the point $z = E_t^1 = -2.46$ mK corresponding to the energy of the trimer excited state, even though this energy does not belong to Π^S. The point is that the position of the pole of the $S_0(z)$-function is determined only by the position of the root of the determinant of the system of linear algebraic equations we solved, whereas the inhomogeneous term of the system plays no role. Therefore, the search for the poles of the grid function $S_0(z)$ is equivalent to the search for the trimer binding energies. The grids we have used turn out to be quite sufficient for this purpose. The convergence of our results for E_t^1 with respect to the parameters N_θ, N_ρ, and $\rho_{\max}$ and their accuracy can be judged from the values of the difference $\epsilon_d - E_t^1$ obtained while using different grids.

Following [9, 15–17], instead of the initial potential $V(x) = V_{\text{HFD-B}}(x)$, we consider the potential

$$V(x) = \Lambda V_{\text{HFD-B}}(x).$$

To establish the mechanism of creating new excited states in He_3 [9, 10], we have calculated the scattering matrix $S_0(z)$ for $\Lambda < 1$. We have found [9] that for a value of Λ slightly smaller than 0.990, the closest to the real axis quasiresonance appeared and transformed into the second-order virtual level [the root of $S_0(z)$] corresponding to the energy value where the graph of $S_0(z)$, $z < \epsilon_d$ is tangent to the z-axis. This virtual level is preceded by the quasiresonances

$$\begin{aligned}
&z = (-1.05 + i\,0.12)\ \text{mK} \qquad \left(\frac{z}{|\epsilon_d|} = -1.59 + i\,0.17\right) \qquad \text{for} \qquad \Lambda = 0.990,\\
&z = (-.99 + i\,0.05)\ \text{mK} \qquad \left(\frac{z}{|\epsilon_d|} = -1.59 + i\,0.64\right) \qquad \text{for} \qquad \Lambda = 0.989.
\end{aligned}$$

The originating virtual level is of the second order, since simultaneously with the root of the $S_0(z)$ function the conjugate root of the function also appears on the real axis. With subsequent decrease of Λ, the second-order virtual level splits into a pair of first-order virtual levels E_t^{2*} and E_t^{2**}, $E_t^{2*} < E_t^{2**}$, which move in opposite directions.

The virtual level E_t^{2**} moves towards the threshold ϵ_d and meets it at $\Lambda < 0.989$. For $\Lambda = 0.975$, the $S_0(z)$ function no longer has any root corresponding to E_t^{2**}. Instead of a root, it acquires a new pole corresponding to the second excited state of the helium trimer with energy E_t^2. Note that, although the virtual levels E_t^{2*} and E_t^{2**} appear beyond the Π^S-domain, already at $\Lambda = 0.985$ the point E_t^{2**} turns out to be inside this domain. Therefore, it should be considered as a true virtual level of the trimer, and we expect that the subsequent Efimov states originate from the virtual levels precisely according to the same scheme as the level E_t^2 does.

The other purpose of the investigation presented is to determine the mechanism of disappearance of the excited state of the helium trimer when the two-body interactions become stronger owing to the increasing coupling constant $\Lambda > 1$. It turned out that this disappearance proceeds precisely according to the scheme of formation of new excited states, but the order of the events occurring is reverse.

The results of calculations [9] of the E_t^1-energy for λ varying from 1.00 to 1.20 are the following. In the interval between $\Lambda = 1.17$ and $\Lambda = 1.19$, there is a jump or irregularity of the behavior of the E_t^1-level on the nonphysical energy sheet and it transforms from the pole of the $S_0(z)$-function into the root, with E_t^{1*} corresponding to the trimer virtual level. For all values Λ [9], the dimer has the bound state only, and the first excited state of the dimer appears at $\Lambda = 6.8$.

Note that, in the case of finite potentials, the geometric characteristics of the Π^S-domain [where the $S_0(z)$ function can be calculated reliably] are determined only by the value of $|\epsilon_d(\Lambda)|$ (9). When $|\epsilon_d(\Lambda)|$ increases, the Π^S-domain is enlarged. It is easy to check that the energies of the excited-state level $E_t^1(\Lambda)$ and of the virtual level $E_t^{1*}(\Lambda)$ belong to the corresponding $\Pi^S(\Lambda)$-domain. For $\Lambda > 1$, this results in a weak dependence of the calculated values of $E_t^1(\Lambda)$ and $E_t^{1*}(\Lambda)$ on the parameters N_θ, N_ρ, and, what is especially important, on the parameter $\rho_{\max}$.

In particular, we chose [9, 10] the values of the cut-off hyperradius $\rho_{\max}$ from the scaling consideration and, as a matter of fact, we took the value of $\rho_{\max}$ following the formula

$$\rho_{\max} = \frac{C}{\sqrt{|\epsilon_d(\Lambda)|}} \qquad \text{with} \qquad C = \sqrt{|\epsilon_d(\Lambda)|}\,\rho_{\max}\,|_{\Lambda=1}\ .$$

Usually $\rho_{\max}$ is equal to 800 Å as was mentioned above.

The ground state of the He_3 system in the three-body approximation is much smaller than that of the He_2 system. However, the value ~ 110 a.u for the excited state is much larger (see Tables 1–5); it is larger than the effective range of the two-body interaction but smaller than the size (200 a.u.) of the scattering length. These relations are a characteristics of any Efimov state.

The results of calculating the scattering states are presented in Figs. 8–11. The phase-shift curves for scattering of the helium atom on the helium molecule are plotted in Figs. 10 and 11 for pairwise potentials both in the BCM approximation (Fig. 11) and without the BCM approximation (Fig. 10), below and above the break-up threshold as well. The energy $E = 1.4$ mk is above the three-body threshold and the break-up amplitudes for this energy are presented in Figs. 8 and 9. The corresponding physical break-up amplitudes $\mathcal{A}_{ll0}(\theta)$, $l = 0, 2$, determined as

$$\mathcal{A}_{aL}(\theta) = A_{aL}(\theta) + \sum_{a'} \int_{-1}^{1} h_{aa'}^{L}(x, y, \eta) A_{a'L}(\theta)\ d\eta,$$

are plotted in Fig. 9 for the HFD-B potential. The shape of the curves is practically the same as for the other type of pairwise potentials mentioned above.

4. Conclusion

Calculations of the scattering and bound states of He_3 were performed using the most advanced few-body calculation techniques both in the BCM approximation and without the BCM approximation. In all the pairwise potentials considered, only two bound states were provided, but the properties of these states appear to be fairly different

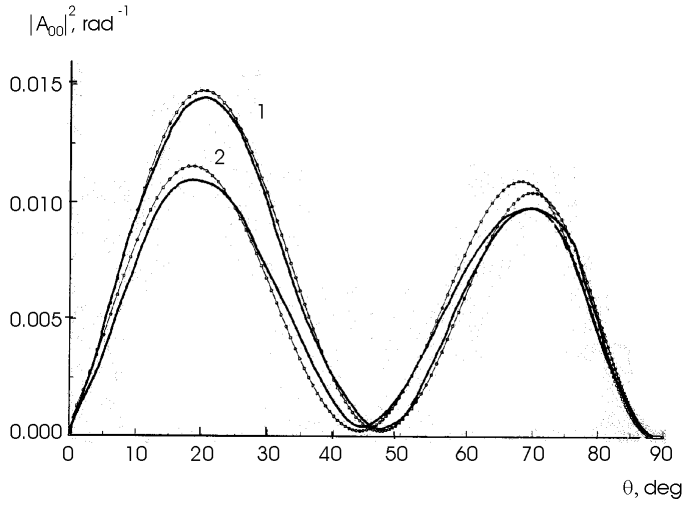

Fig. 8. Modulus squared of the Faddeev break-up amplitude $A_{00}(\theta)$ for the HFD-B potential at $E = +1.4\,\mathrm{mK}$ in the BCM approximation. Curve 1 corresponds to the partial wave with $L = 0$, $l = \lambda = 0$. Curve 2 was obtained with inclusion of $L = 0$, $l = \lambda = 2$. Solid curves correspond to calculations without the BCM approximation.

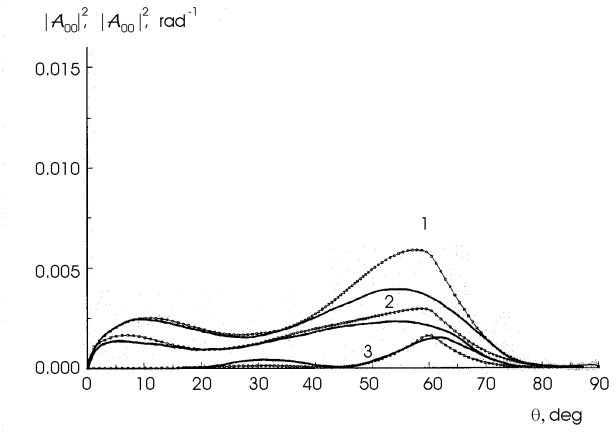

Fig. 9. Modulus squared of the physical break-up amplitudes $\mathcal{A}_{00}(\theta)$ (curves 1 and 2) and $\mathcal{A}_{22}(\theta)$ (curve 3) for the HFD-B potential at $E = +1.4\,\mathrm{mK}$ in the BCM approximation. Curve 1 corresponds to inclusion of $L = 0$, $l = \lambda = 0$ only, while curves 2 and 3 were obtained with inclusion of both $l = \lambda = 0$ and $l = \lambda = 2$ partial waves. Solid curves correspond to calculations without the BCM approximation.

(1) the ground state is strongly bound, whereas the binding energy of the excited state is comparable with the dimer binding energy;

(2) the sizes of these two states are fairly different.

The characteristic size of the ground state was estimated as $\langle r \rangle$ or $\langle r^2 \rangle^{1/2}$ and it is approximately 10 times smaller than the size of the dimer molecule, but the size of the excited state has the same order of magnitude as the dimer.

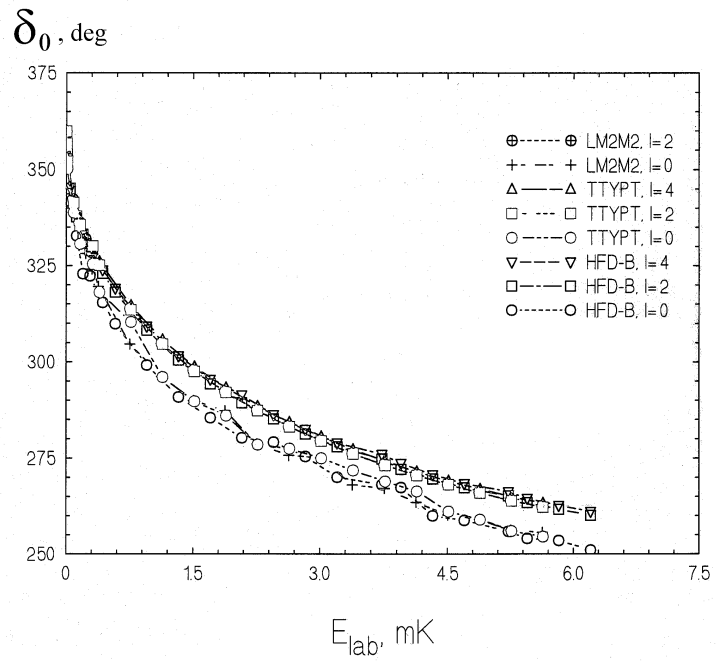

Fig. 10. Scattering phase shifts $\delta_0(E_{\rm lab})$, $E_{\rm lab} = \frac{3}{2}(E+|\epsilon_d|)$, for S-wave He–$He_2$ collisions for the HFD-B, LM2M2, and TTYPT potential.

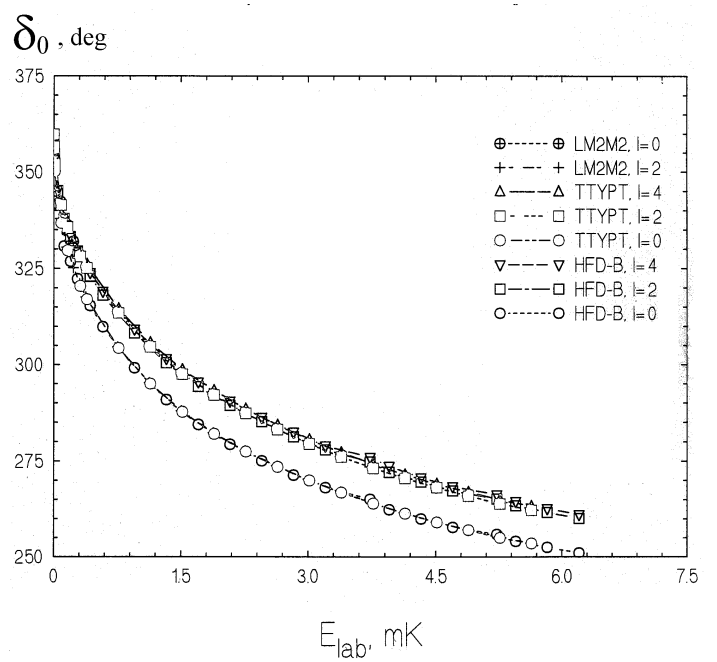

Fig. 11. Scattering phase shifts $\delta_0(E_{\rm lab})$, $E_{\rm lab} = \frac{3}{2}(E+|\epsilon_d|)$, for S-wave He–$He_2$ collisions for the HFD-B, LM2M2, and TTYPT potential (BCM approximation).

Acknowledgments

This work was supported by the Ministry of Science and Technology of the People's Republic of China, the Chinese National Science Foundation (19734030), the National Scientific Council of the Republic of China (Taiwan) under Project NSC 85-212-M-007-009, and the Russian Foundation for Basic Research under Projects Nos. 98-02-17266 and 01-02-16075.

References

1. V. Efimov, *Nucl. Phys.* A, **362**, 45 (1981); **378**, 581 (1982); *Phys. Rev.* C, **47**, 1876 (1993); S. A. Vugalter and G. M. Zislin, *Theor. Math. Phys.*, **7**, 332 (1971); **32**, 7 (1977); *Dokl. AN USSR*, **267**, 784 (1982).
2. L. D. Faddeev and S. P. Merkuriev, *Quantum Scattering Theory for Several-Particle Systems*, Kluwer Academic, London (1993).
3. D. V. Fedorov, A. S. Jensen, and K. Rusager, *Phys. Rev.* C, **50**, 2372 (1994); *Phys. Rev. Lett.*, **82**, 2844 (1999).
4. A. Cobis, D. V. Fedorov, and A. S. Jensen, *Phys. Lett.* B, **424**, 1 (1998).
5. J. Yuan and C. D. Lin, *J. Phys.* B, **31**, L637 (1998).
6. T. Gonzalez-Lezana, J. Rubayo-Soneira, S. Miret-Aztes, et al., *J. Chem. Phys.*, **110**, 1648 (1999); *Phys. Rev. Lett.*, **82**, 1648 (1999).
7. A. R. Janzen and R. A. Aziz, *J. Chem. Phys.*, **103**, 22, (1995).
8. K. T. Tang, J. P. Toennies, and C. L. Yiu, *Phys. Rev. Lett.*, **74**, 1546 (1995).
9. A. K. Motovilov, E. A. Kalganova, and S. A. Sofianos, *J. Phys.* B, **31**, 1279 (1998); *J. Chem. Phys.*, **275**, 168 (1997); *Phys. Rev.* A, 56, R1686 (1997).
10. V. Rudnev, and S. Yakovlev, *Chem. Phys. Lett.*, **22**, 97 (2000); *Phys. Atom. Nucl.*, **63**, 61, 77, 271, 278, 402, 409, 830 (2000).
11. T. Frederico, Lauro Tomio, A. Delfino, et al., *Phys. Rev.* A, **60**, R9 (1999).
12. Y. Hahn, *Phys. Rev.* A, **60**, 2139 (1999).
13. E. Nielsen, D. V. Fedorov, and A. S. Jensen, *Phys. Rev. Lett.*, **82**, 2844 (1999).
14. P. F. Bedaque, H. W. Hammer, U. van Kolek, *Phys. Rev. Lett.*, **82**, 463 (1999).
15. R. A. Ionescu and C. Nategan, *Europhys. Lett.*, **45**, 269 (1999).
16. S. P. Merkuriev and S. A. Pozdneev, *Sov. J. Nucl. Phys.*, **29**, 620 (1979).
17. S. A. Pozdneev, "Application of quantum theory of scattering to the calculation of various processes in atomic, molecular, and nuclear physics," in: *Dynamics of Elementary Atomic-Molecular Processes in Gas and Plasma*, *Proceedings of the P. N. Lebedev Physical Institute*, Nova Science, New York (1996), Vol. 212, p. 99.
18. S. Pozdneev, *Phys. Lett.* B, **125**, 355 (1983).
19. A. R. Janzen and R. A. Aziz, *J. Chem. Phys.*, **79**, 4330 (1979); **94**, 8047 (1991); **103**, 9626 (1995); *Mol. Phys.*, **61**, 1487 (1987); S. Pozdneev, "The method of determination of potential energy curves of diatomic molecules and their ions," in: *Laser Chemistry, Biophysics and Biomedicine, ICONO'95*, Plenum Publishers, New York (1996), p. 92; *Physics-Lebedev Institute Reports*, Nos. 1–2, 61 (1997); H. Magenan and N. R. Kestner, *Theory of Intermolecular Forces*, Pergamon, New York (1971); W. J. Meath, D. J. Margoliash, B. L. Jhanwar, et al., *Intermolecular Interactions: From Diatomics to Biopolymers*, Wiley-Interscience Publishers, London (1978); J. N. Mirrell, S. Carter, S. C. Faran-

tos, et al., *Molecular Potential Energy Functions*, John Wiley & Sons, New York (1984); N. Sathyamurthy, *Computer Phys. Rep.*, **3**, 4 (1985).
20. K. P. Huber and G. Herzberg, *Constants of Diatomic Molecules*, Plenum Press, New York (1979).
21. L. V. Kantorovich and V. I. Krilov, *Approximate Methods of Mathematical Analysis* [in Russian], Fizmatgiz, Moscow (1962).
22. F. Lon, C. F. Giese, and W.R. Gentry, *J. Chem. Phys.*, **104**, 1151 (1996); W. Schollkopf and J. P. Toennies, *J. Chem. Phys.*, **104**, 1155 (1996); M. V. Rama Krishna and K. V. Whaley, *Phys. Rev. Lett.*, **64**, 1126 (1990); G. C. Hegerfeldt and T. Kohler, *Phys. Rev.* A, **57**, 2021 (1998); **61**, 3606 (2000); *Phys. Rev. Lett.*, **84**, 3215 (2000).